On the decay of strength in Guilin red clay with cracks

Yi Li, Keneng Zhang
School of Geosciences and Info-Physics, Central South University, Changsha, 410083, China
349613828@qq.com

Baochen Liu
College of Civil Engineering and Architecture, Guilin University of Technology, Guilin, 541004, China
979811051@qq.com

Zongyuan Pan
Institute of Karst Geology, CAGS, Guilin, 541004, China
65709162@qq.com

ABSTRACT. In order to research the effect of cracks in red clay on shear strength through dry-wet cycle test, the experimenters used imaging software and a mathematical model to determine fractal dimension and crack ratio of surface cracks in red clay in Guilin, China. After each dry-wet cycle, direct shear tests were carried out on the sample, and such variables as matrix suction on the crack propagation process of red clay were analyzed. The mechanics model was established and obtained the critical condition of soil cracks. The results show that with the increase in the number of dry-wet cycles the shear strength of the samples would decrease. But the rule of shear strength of sample 3 is slightly different from samples 1 and 2. The shear strength of red clay has a good correlation with fractal dimension and crack ratio, which could be an identification index of the strength of red clay.

KEYWORDS. Red clay; Dry-wet cycle; Fractal dimension; Crack ratio; Shear strength.

INTRODUCTION

Guilin is located in the northeast of Guangxi Province, at a low latitude, with a subtropical monsoon climate. It is variably rainy throughout the year, with the rainy season coinciding with high temperatures. The climate easily causes the development of soil fissure of Guilin red clay resulting in a decline in the ultimate strength of the clay. We should pay attention to the influence of red clay cracks on the stability in the area of slope and foundation excavation, as it may lead to free face collapse, ground subsidence and other geological mishaps. Therefore, researching the influence of cracks on the shear strength of red clay will help us to improve the safety of the geo-body. Cracks in soil have been a concern for a long time, however, the research on geotechnical engineering is still relatively insufficient. Until the 1980s, only a few scholars have started the research on the soil cracks [1-6].

A new kind of constitutive model capable of describing the damage of soil structure has been proposed and crack evolution in clay during dry and wet cycles has been simulated [7,8]. The effects of cyclic dry-wet process on the fatigue

strength of the cement silt clay and the cement silt were researched by cyclic triaxial tests [9]. High liquid limit undisturbed clay quick shear tests with different moisture were carried out through different dry-wet cycle paths, including the process of humidification and dehumidification of the dry-wet cycle[10]. The relationship between particle mesoscopic and macroscopic mechanical parameters of cohesive materials were studied [11]. But there is little research on shear strength of red clay based on dry-wet cycle. Experiments have been conducted on the strength characteristics of unsaturated red clay and expansive soil, which are different from those of common clay soil [12]. The relationships among mechanical indexes, swelling-shrinkage properties, pore size distributions and moisture content of lateritic clay in Guigang of Guangxi Zhuang Autonomous Region were discussed [13]. The red clay soil and the expansive soil were analyzed regarding the relationships between shear strength index and temperature [14]. It has been determined that high and low confining pressures have different effects on the deformational properties and mechanical index of frozen soil [15]. In addition, the above results show the various impact factors of study on intensity variability of the clay. However, the cracks' effect on the shear strength of red clay has been limited.

In order to observe development of red clay fractures, we simulated red clay in dry-wet cycles under natural conditions combined with computer image processing technology. It was concluded that reticular cracks will form in the red clay under certain circumstances, then a direct shear apparatus was used to test this sample. The test considered multiple factors in controling the cutting ring size and humidification method to determine the fractal dimension and crack ratio of three samples under different conditions. After each dry-wet cycle, direct shear tests were conducted on samples to study the effects of red clay cracks on cohesive force and internal friction angle.

TESTING METHODS

Samples

The red clay samples were taken from the Guilin Yan Mountain. The red clay samples were dried then crushed, and a fine sieve 2.0mm was used to sieve samples. Finally, these samples were stored. The physical and mechanical parameters of the red clay are shown in the Tab. 1.

w/%	ϱ(g/cm³)	e	I_P/%	I_L	c/kPa	φ /°	a_{v1-2}/MPa^{-1}
51.20	1.81	1.42	26.10	0.76	19.00	13.20	0.60

Table 1: Physical and mechanical indexes of red clay.

Factors	Value	Class Number
Artificial humidification	Times of dry-wet cycle: 1, 2, 3, 4, 5; Moisture content: 35%; Dry density: 1.5 g/cm³; Small cutting ring: diameter is 61.8mm, height is 20mm; Large cutting ring: diameter is 150mm, height is 50mm.	Small cutting ring: 12 group Large cutting ring: 12 group
Vacuum saturation	Times of dry-wet cycle: 1, 2, 3, 4, 5; Moisture content: 35%; Dry density: 1.5 g/cm³; Small cutting ring: diameter is 61.8mm, height is 20mm.	Small cutting ring: 12 group

Table 2: Test project.

Test project

This test mainly considered the sample size and the influence of different humidification methods on the mechanical properties of red clay. Study on the attenuation law of shear strength of samples after five dry-wet cycles shows that shear

strength is related to fractal dimension and crack rate, according to the design scheme carried out by the direct shear test. One type of the sample's diameter is 61.8mm and the height is 20mm, another sample's diameter is 150mm and the height is 50mm. A drying cabinet set at 60°C was used to dehydrate all of these samples for 12h. The wet mode was divided into two methods; artificial humidification (using a watering can to spray distilled water onto the surfaces of the obtained samples for 10 minutes, then putting the samples in cylinder seals for 24h) and vacuum saturation (pumping gas saturation for 1h, then soaking the samples in water for 10h). The specific plan is shown in the Tab. 2.

FRACTURE DEVELOPMENT MECHANISM ANALYSIS

Fracture characterization analysis

This paper selects the artificial humidification using a small cutting ring (sample 1) and a large cutting ring (sample 2) and vacuum saturated (sample 3) for each group, respectively. The article determines fractal dimension and crack ratio of three groups of samples in five dry-wet cycles (see Tab. 3). The crack ratio is determined by the use of Matlab to select and count black and white pixels of the image, then is compared with the amount of black pixels in general pixels by the following formula,

$$\delta = \frac{fracture\ area}{surface\ area} \times 100\% = \frac{black\ \ pixels}{general\ \ pixels} \times 100\% \tag{1}$$

The fractal dimension of the crack is measured by determining the box dimension. The box dimension is defined as coordinates net δ of R^n: $[m_1, (m_1+1)] \times \cdots \times [m_n, (m_n+1)]$, $[m_i, (m_i+1)]$ is the side of coordinates net δ, $m_1, \cdots, m_n$ are integers.

Suppose F is a limited non-zero collection on R^n, $N_\delta(F)$ stands for diameter, the maximum δ can cover a minimum set number, the box dimension for F is defined as:

$$\underline{Dim}_B F = \underline{lim}_{\delta \to 0} \frac{logN_\delta(F)}{-log\delta} \tag{2}$$

$$\overline{Dim}_B F = \overline{lim}_{\delta \to 0} \frac{logN_\delta(F)}{-log\delta} \tag{3}$$

When the dimensions of the upper box and the lower box are equal, F is called the box dimension, indicated as:

$$Dim_B F = lim_{\delta \to 0} \frac{logN_\delta(F)}{-log\delta} \tag{4}$$

When calculating the box dimension for F, the length of δ intersects F, and the number of the intersectional points is the box dimension $N_\delta(F)$. When δ approaches zero, this means adding logarithmic speed of $N_\delta(F)$, or the negative values of the slopes of log δ and $\log N_\delta(F)$ is the box dimension.

The box dimension of the red clay crack can be determined as follows: in order to calculate its box dimension, the images of cracks are regard as a set F. We can draw a square grid of coordinate δ in the image to calculate F and grid square intersect number $N_\delta(F)$, take the value of δ (for example, $n=1/2^n$, n=1, 2,...), then confirm the different $N_\delta(F)$. In this region, by using the least square method we can get the regression linear equation:

$$gN_\delta(F) = a(lg\delta^{-1}) + b \tag{5}$$

The slope of the linear can be regarded as approximate value of box dimension F, based on the box-counting dimension, the box dimension of crack image under various δ can be obtained:

$$dim_B f_{\delta_n} = \frac{lgN_{\delta_n}(f)}{lg\delta_n^{-1}} \tag{6}$$

Number of dry-wet cycles:		1	2	3	4	5
Sample 1	Crack ratio	0	1.65%	2.57%	3.27%	3.63%
	Fractal dimension	0	0.632	0.783	1.012	1.133
Sample 2	Crack ratio	2.25%	2.77%	3.86%	6.55%	8.03%
	Fractal dimension	0.688	0.853	1.016	1.193	1.417
Sample 3	Crack ratio	0	2.14%	2.92%	3.37%	3.77%
	Fractal dimension	0	0.963	1.076	1.167	1.257

Table 3: Number of dry-wet cycles as related to crack ratio and fractal dimension.

Tab. 3 shows that sample 1 and sample 3 had no fissures after the first wet-dry cycle, but the crack ratio and fractal dimension were 2.25% and 0.688, respectively. Comparing three groups of crack samples after five dry-wet cycles, the fissure of sample 2 developed earlier and more was more substantial than that of samples 1 and 3. This is because sample 2 was obtained by the large ring sampler while samples 1 and 3 used the small ring. In addition, the fissure ratio and fractal dimension of sample 3 was slightly larger than that of sample 1 due to different humidification methods.

Fracture mechanical analysis

The red clay is the unsaturated soil under normal circumstances. This soil has the characteristics of shrinkage and the rate of water loss in soil on the surface is greater than internally. After water loss and the matric suction increases, the soil is subjected to tensile stress at first.

Assuming that the soil is isotropic and linear elastic bodies, the following constitutive relations can be established:

$$\begin{cases} \varepsilon_x = \dfrac{\sigma_x - u_a}{E} - \dfrac{\mu}{E}\left(\sigma_y + \sigma_z - 2u_a\right) + \dfrac{u_a - u_w}{H} \\ \varepsilon_y = \dfrac{\sigma_y - u_a}{E} - \dfrac{\mu}{E}\left(\sigma_x + \sigma_z - 2u_a\right) + \dfrac{u_a - u_w}{H} \\ \varepsilon_z = \dfrac{\sigma_z - u_a}{E} - \dfrac{\mu}{E}\left(\sigma_x + \sigma_y - 2u_a\right) + \dfrac{u_a - u_w}{H} \end{cases} \tag{7}$$

where

u_a - pore air pressure

u_w - pore water pressure

E - elastic modulus of soil

μ - poisson ratio

H - elastic modulus associated with $u_a - u_w$,

ε_x - horizontal strain

ε_y - longitudinal strain

ε_z - vertical strain

σ_x - horizontal stress

σ_y - longitudinal stress

σ_z - vertical stress.

Taking the horizontal as the object of study, and there are no cracks in the soil:

$$\varepsilon_x = 0 \tag{8}$$

The first combination of the constitutive relation:

$$\sigma_x - u_a = \frac{\mu}{1-u}\left(\sigma_z - u_a\right) - \frac{\left(u_a - u_w\right)E}{H\left(1-u\right)} \tag{9}$$

When the matrix suction is zero, the soil pressure formula is expressed as a saturated state. In the unsaturated soil, the matrix suction can decrease the horizontal stress, and even with a negative matrix suction it will form tension stress. When tensile stress is greater than the ultimate strength of soil, cracks will appear on the surface. The maximum tensile strength of soil is σ_f, criterion condition as follows:

$$\sigma_x - u_a = \frac{\mu}{1-u}\left(\sigma_z - u_a\right) - \frac{\left(u_a - u_w\right)E}{H\left(1-u\right)} \le -\sigma_f \tag{10}$$

At the initial stages of fracture, without considering u_a, we can assume $\sigma_z - u_a \approx 0$, $u_a - u_w \approx S_0$, S_0 is matric suction:

$$\frac{\left(u_a - u_w\right)E}{H\left(1-u\right)} \le \sigma_f \tag{11}$$

Before cracking matric suction is as follows:

$$S_0^f = \left(u_a - u_w\right) \le \frac{\sigma_f H\left(1-\mu\right)}{E} \tag{12}$$

In the isotropic linear elastic soil, $E/H = \left(1-2\mu\right)$, by the following formula:

$$S_0^f = \frac{\sigma_f\left(1-\mu\right)}{\left(1-2\mu\right)} \tag{13}$$

The critical condition of soil crack:

$$S_0 \ge S_0^f = \frac{\sigma_f\left(1-\mu\right)}{\left(1-2\mu\right)} \tag{14}$$

RESULTS

The relationship between shear strength and wet-dry cycle

(1) The relationship between the number of dry-wet cycles and cohesive force is shown in Tab. 4 and Fig. 1. The cohesive force of samples 1 and 2 have essentially the same tendency for chang, and with the increase of the number of dry-wet cycles the cohesive force would decrease. After the first wet-dry cycle, the maximum cohesion of samples 1 and 2 are 39.38kPa and 38.57kPa, respectively. Sample size has no effect on the trend of the cohesion of red clay, but the method of humidification has a significant impact on cohesion, meaning that after five wet-dry cycles, the cohesion of sample 3 decreases.

(2) The relationship between the number of dry-wet cycles and internal friction angle is shown in Tab. 4 and Fig. 2. The internal friction angle and cohesion of samples 1 and 2 have essentially the same tendency for chang, but the internal friction angle of sample 2 is generally greater than that of sample 1, so sample size has significant effects on the internal friction angle. After two dry-wet cycles, the internal friction angle of sample 3 drops little, but after the third wet-dry cycle, the internal friction angle drops rapidly, the minimum value being 6.68°, so vacuum saturation has greater effect on the internal friction angle of samples than artificial humidification.

The relationship between shear strength and crack ratio

(1) The relationship between cohesive force and crack ratio is shown in Tab. 5 and Fig. 3. With crack ratio increasing the cohesive force of samples would decrease, but the reducing tendency shows little difference. When the crack

ratios of samples 1, 2 and 3 are over 1.65%、2.77% and 2.14% respectively, the cohesion drops rapidly, which indicates that there is a threshold quantity that makes the cohesion of red clay change. The cracks of sample 2 appears earlier than those of samples 1 3. After five dry-wet cycles, the cohesion of samples 1 and 2 are about 19kPa, but the cohesion of sample 3 is only 13.77kPa.

(2)

Number of dry-wet cycles:		1	2	3	4	5
Sample 1	Cohesive force / kPa	39.38	38.21	36.14	29.57	19.05
	Internal friction angle /°	8.82	8.56	8.49	7.88	7.26
Sample 2	Cohesive force / kPa	38.57	37.89	34.77	30.09	18.66
	Internal friction angle /°	9.76	9.29	9.03	8.56	7.12
Sample 3	Cohesive force / kPa	38.04	33.05	27.39	19.33	13.77
	Internal friction angle /°	9.06	8.66	7.69	7.13	6.68

Table 4: The relationship between the number of dry-wet cycles and shear strength of test results.

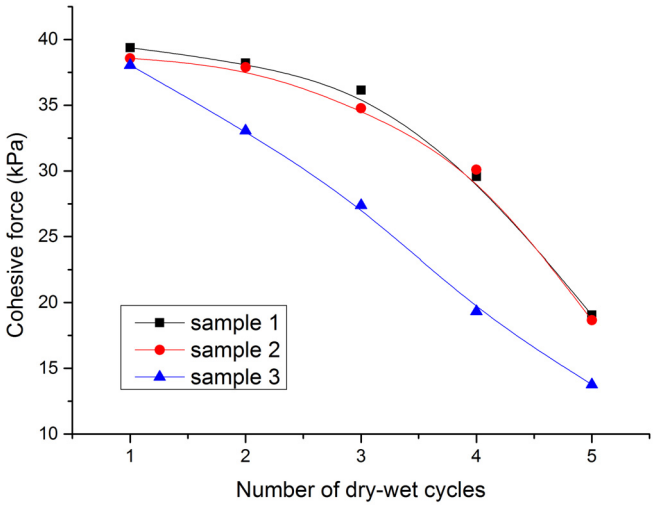

Figure 1: The relationship between the number of dry-wet cycles and cohesive force.

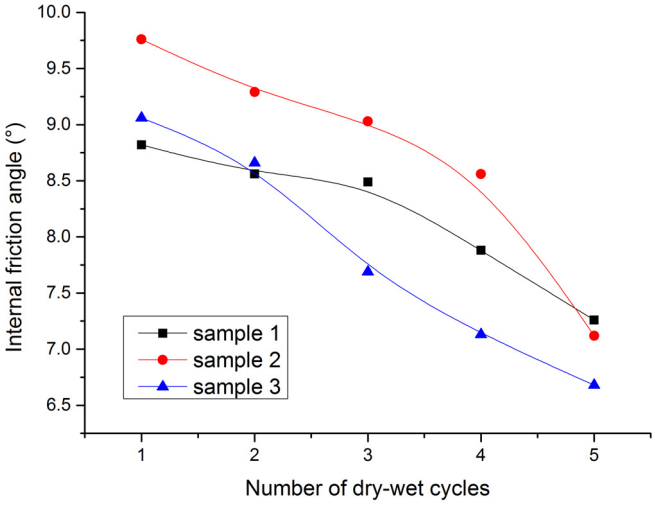

Figure 2: The relationship between the number of dry-wet cycles and internal friction angle.

(2) The relationship between the crack ratio and the internal friction angle is shown in Tab. 5 and Fig. 4. Changes in the internal friction angle in different crack ratios are familiar to cohesive force, both having a threshold quantity. After two dry-wet cycles, the internal friction angle of sample 3 is slightly higher than that of sample 1, but after the forth wet-dry

cycle, the law reverses. After the first dry-wet cycle, the internal friction angle of sample 2 is 9.76° , the largest of the three samples.

Number of dry-wet cycles:		1	2	3	4	5
Sample 1	Crack ratio	0	1.65%	2.57%	3.27%	3.63%
	Fractal dimension	0	0.632	0.783	1.012	1.133
	Cohesive force / kPa	39.38	38.21	36.14	29.57	19.05
	Internal friction angle /°	8.82	8.56	8.49	7.88	7.26
Sample 2	Crack ratio	2.25%	2.77%	3.86%	6.55%	8.03%
	Fractal dimension	0.688	0.853	1.016	1.193	1.417
	Cohesive force / kPa	38.57	37.89	34.77	30.09	18.66
	Internal friction angle /°	9.76	9.29	9.03	8.56	7.12
Sample 3	Crack ratio	0	2.14%	2.92%	3.37%	3.77%
	Fractal dimension	0	0.963	1.076	1.167	1.257
	Cohesive force / kPa	38.04	33.05	27.39	19.33	13.77
	Internal friction angle /°	9.06	8.66	7.69	7.13	6.68

Table 5: Test results of the relationship between crack ratio, fractal dimension and shear strength.

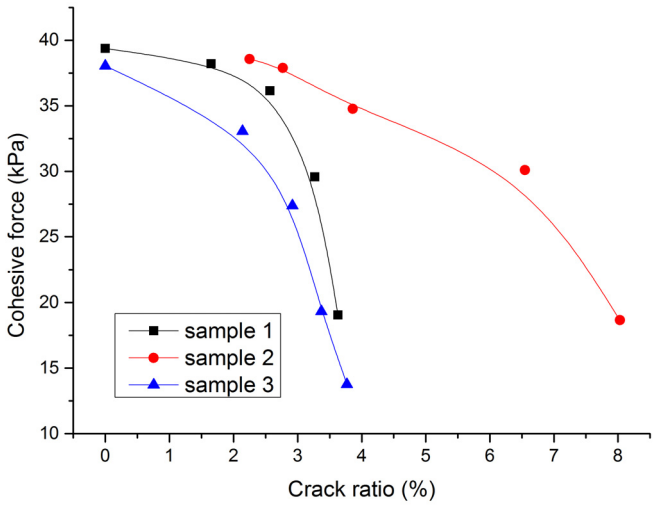

Figure 3: The relationship between crack ratio and cohesive force.

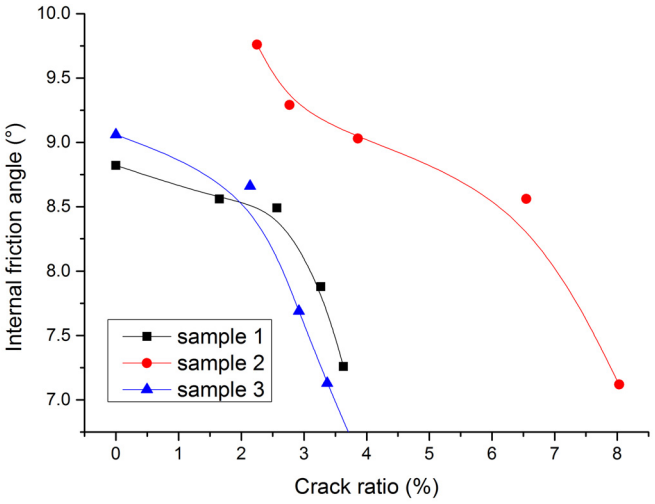

Figure 4: The relationship between crack ratio and internal friction angle.

The relationship between shear strength and fractal dimension

(1) The relationship between fractal dimension and the cohesive force is shown in Tab. 5 and Fig. 5. With fractal dimension increasing, the cohesive force would decrease. When the fractal dimensions of samples 1, 2 and 3 are over 0.5, 0.85 and 0.963 respectively, the cohesion drops rapidly, and changes of cohesion in different fractal dimensions are familiar to crack ratio. But even though the mutation of the fracture in sample 3 is apparent, it cannot be observed when the fractal dimension is less than 0.963, so it is considered to have no impact on crack ratio in this situation.

(2) The relationship between the fractal dimension and the internal friction angle is shown in Tab. 5 and Fig. 6. Changes in the internal friction angle in different fractal dimensions are familiar to cohesive force, and they both have a threshold quantity. After the first wet-dry cycle, the crack of samples 1 and 3 do not appear, the fractal dimension is 0, the internal friction angle is 8.82°and 9.06°respectively. After the second wet-dry cycle, because of the different method of humidification, the fractal dimension and internal friction angle of samples 1 and 3 have different trends. Due to the relatively large size, sample 2 would form the earlier fracture, with the fractal dimension having a great effect on the internal friction angle.

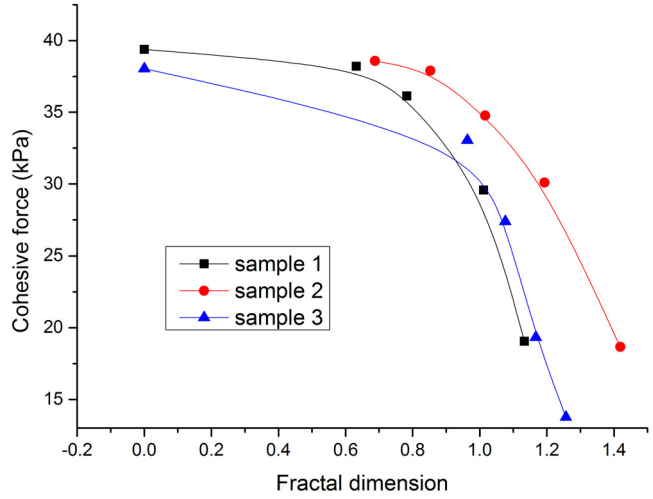

Figure 5: The relationship between fractal dimension and cohesive force.

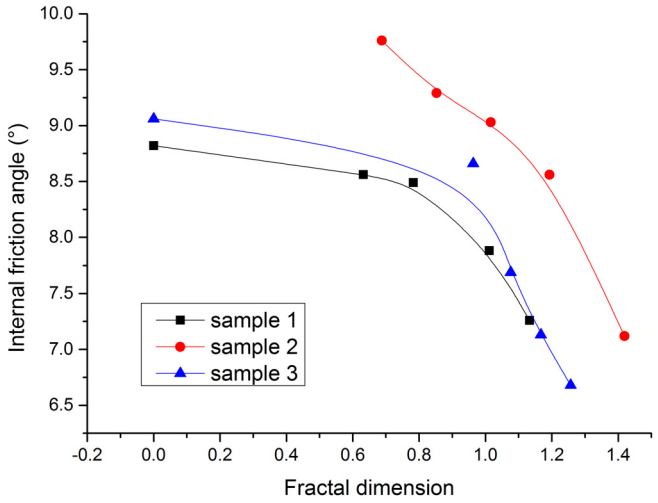

Figure 6: The relationship between fractal dimension and internal friction angle.

CONCLUSION

By changing the sample size and humidification method to study the effects of cracks on shear strength of red clay, this study analyzed the mechanics of red clay cracking, and the main conclusions are as follows:

1. To analyze variables such as the matrix suction in the process of fracture development in red clay, we established the mechanics model, determined the state equation of the soil cracking critical conditions, so that study of the images of soil fissures would become an analysis of the specific formula.

2. With the increase of the number of dry-wet cycles, shear strength of samples 1 and 2 would decrease. After the first dry-wet cycle, the intensity index was at its maximum. With the increase of the number of dry-wet cycles, the cohesive force of sample 3 continued to decline.

3. There is a strong correlation between the shear strength of red clay and the crack ratio. With an increase in the crack ratio, the strength curve of samples 1 and 3 are both similar to a parabola, and the change rule of the curve of sample 2 is slightly different.

4. With an increase in the fractal dimension, the intensity index will decrease, as the influence of the crack ratio on the strength index shows that the fractal dimension can be used as one of the indicators in discrimination of the crack influence on the strength of red clay.

REFERENCES

[1] Yingwen, Z., Lingwei, K., Aiguo, G., et al., Mechanical behaviors and water-sensitive properties of intact Guangxi laterite, Rock and Soil Mechanics, 04 (2003) 568-572.

[2] Zhihong, H., Lijun, Z., Yiling, L., et al., Study on mechanical properties of red clay fracture, Geotechnical Investigation and Surveying, 4 (2004) 9-12.
[3] Zhiwei, W., Gengsun, W., FLAC simulation for progressive failure of fissured clay slope, Rock and Soil Mechanics, 10 (2005) 116-119.
[4] Morris, P.H., Graham, J., Williams, D.J., Cracking in Drying Soils, Can Geotech. J., 29 (1992) 264-277.
[5] Konrad, J.M., Ayad, R., Desiccation of a sensitive clay: field experiment observations, Can Geotech.J., 34 (1997) 929-942.
[6] Preston, S., Griffiths, B.S., Young, I.M., An investigation into sources of soil crack heterogeneity using fractal geometry, European Journal of Soil Science, 48 (1997) 31-37.
[7] Zhujiang, S., A masonry model for structured clays, Rock and Soil Mechanics, 01 (2000) 1-4.
[8] Zhujiang, S., Gang, D., Numerical simulation of crack evolution in clay during drying and wetting cycle, Rock and Soil Mechanics, S2 (2004) 1-6.
[9] Minglong, Z., Jianhua, W., Aihua, L., Test study on the effect of cyclic dry—wet process on the fatigue strength of cement-soil, China Railway Science, 02 (2005) 28-31.
[10] Jinlai, Y., Tian, H., Jian, Z., et al., Change of high liquid limit clay intensity during humidification and dehumidification process of the dry-wet cycle, Journal of Changsha University of Science and Technology (Natural Science), 03 (2011) 39-43.
[11] Bo, Z., Huabin, W., Wenfeng, Z., et al., Analysis of relationship between particle mesoscopic and macroscopic mechanical parameters of cohesive materials. Rock and Soil Mechanics, 10 (2012) 3171-3175.
[12] Qing, Y., Jie, H., Maotian, L., Comparative study on shear strength of unsaturated red clay and expansive soils, Rock and Soil Mechanics, 01 (2003) 13-16.
[13] Yingwen, Z., Ling-wei, K., Aiguo, G., et al., Strength properties and swelling-shrinkage behaviors of compacted lateritic clay in Guangxi, Rock and Soil Mechanics, 03 (2004) 369-373.
[14] Xiaoduo, O., Heng, W., Dong, Z., Comparative study on thermodynamics characteristics of red clay and expansive soils in Guangxi, Rock and Soil Mechanics, 07 (2005) 1068-1072.
[15] Xinglian, S., Ren, W., Mingjian, H., et al., Triaxial strength and deformation properties of frozen silty clay under low confining pressure, Rock and Soil Mechanics, 10 (2005) 102-106.